Complexation of Lead(II) by Chlorogenic Acid: Experimental and Theoretical Study

Jean-Paul Cornard,* Christine Lapouge, Laetitia Dangleterre, and Cyrille Allet-Bodelot

LASIR, CNRS UMR8516, Université des Sciences et Technologies de Lille, Bât C5, 59 655 Villeneuve d'Ascq Cedex, France

Received: June 20, 2008; Revised Manuscript Received: September 29, 2008

Density functional theory (DFT) structure calculations and time-dependent DFT electronic excitation calculations have been performed on chlorogenic acid (H_3CGA), a polyphenolic compound, used as a model molecule of humic substances. The different deprotonated forms of H_3CGA have also been investigated. H_3CGA is a multisite ligand that presents several metal complexing sites in competition, notably the carboxylic and catechol moieties. In low acidic aqueous medium, the complexation of Pb(II) has been followed by electronic absorption spectrometry. The formation of two complexes of stoichiometry metal:ligand 1:1 (log $\beta_{1:1} = 3.39$) and 2:1 (log $\beta_{2:1} = 7.12$) has been highlighted with use of chemometric methods. The theoretical spectrum of the 1:1 complex obtained by TD-DFT methodology shows the formation of a chelate $[Pb(H_2CGA)(H_2O)_3]^+$ with the metal fixation at the level of the carboxylate function. The second complexing site, the catechol moiety, is rapidly involved in the formation of the 2:1 complex from molar ratios [metal]/[ligand] higher than 0.1. The electronic transitions calculated for both free ligand and complexes involved the same molecular orbitals, and no ligand−metal or metal−ligand charge transfer is observed.

1. Introduction

The problem of environmental pollution with heavy metals due to anthropogenic activities is becoming increasingly urgent to the living world. Excessive levels of heavy metals introduced to soil can lead to elevated uptake of these pollutants by plants, which causes damage to plants and affects human health upon consumption of crops grown in the soil. Different forms of heavy metals have different mobility and phytoavailability.[1] Generally, the plant uptake of heavy metals is correlated to extractable forms of the metals rather than to the total metal contents in the soils.[2] Lead is a major pollutant in terrestrial ecosystems. Lead pollution occurs through a variety of activities, including mining, metal processing, battery manufacture and disposal, the burning of leaded fuels, and application of sludge to agricultural land.[3] Indeed, under some circumstances, soils subjected to anthropogenic pollution have been reported to contain Pb concentrations of up to 20 mg/g.[4] Natural organic matter (NOM) plays a significant role in the binding of this toxic metal in the natural environment. NOM is a complex mixture of organic compounds derived mostly from decaying vegetation in the environment.[5,6] Present in soils, but also in sediments and water, these substances have defied molecular-level characterization for nearly a century, owing primarily to the fact that they exist mostly as highly functionalized polyelectrolytes and, as such, do not lend themselves to analytical techniques for molecular characterization. Soluble extracts of NOM can be recovered from soils and sediments by well-established alkaline extraction protocols,[7] and these are referred to as humic substances (HS). The main difficulty in predicting interactions of metal ions with HS is that organic materials exhibit strong chemical heterogeneity. HS can trap metals by van der Waals interactions or by complexation with various potential groups, such as carboxylic, carboxylate, catechol, and hydroxy-carbonyl functions.[8] However, the binding mechanisms for metal cations are not fully understood. To advance understanding of metal−NOM interactions, it is useful to study over a wide range of conditions the complexation of smaller, well-characterized molecules containing the functional groups of HS. While simple organic acids do not possess the complexity of HS, their complexing properties can be remarkably similar to those of the supramolecular structure.[9−12]

Phenolic acids are naturally occurring compounds, omnipresent in the vegetable kingdom, and are at the origin of the HS formation. The amount of phenolic acids (e.g., caffeic, ferulic, gallic, protocatechuic, and chlorogenic acids) is evaluated to be up to 35% of HS, depending of their origin. Chlorogenic acid (5-*O*-caffeoylquinic acid), an ester of caffeic acid with quinic acid, has received considerable attention for its wide distribution and potential biological effects.[13−16] Chlorogenic acid (H_3CGA), a multifunctional natural organic acid, presents several metal fixing sites in competition and has already been used as a model molecule of HS.[17−23] Several papers report the complexing ability of H_3CGA toward different metal ions in aqueous solution, such as iron,[24−26] copper,[18,24,26,27] manganese,[24] zinc,[24,26] and aluminum,[28−32] but to our knowledge the Pb(II)−H_3CGA system has never been studied.

The objective of this paper is to study the Pb(II) complexation by H_3CGA in aqueous solution by jointly using UV−visible absorption spectroscopy and quantum chemical calculations. The methodology, which consists of combining electronic spectroscopy and time-dependent density functional theory (TD-DFT), already proved reliable to identify the preferential fixing site of a metal ion by a multisite ligand.[33−35] In the first step, chlorogenic acid and its different deprotonated forms were theoretically studied to determine their most stable conformation; the spectral features of these ligands were also investigated. Then the complexation reaction of Pb(II) by chlorogenic acid was followed by electronic spectroscopy. The pH of the solution was slightly acidic (pH 6) to be close to the pH generally found in the soils.

* Author to whom correspondence should be addressed. E-mail: jean-paul.cornard@univ-lille1.fr.

10.1021/jp805463p CCC: $40.75
Published on Web 11/08/2008

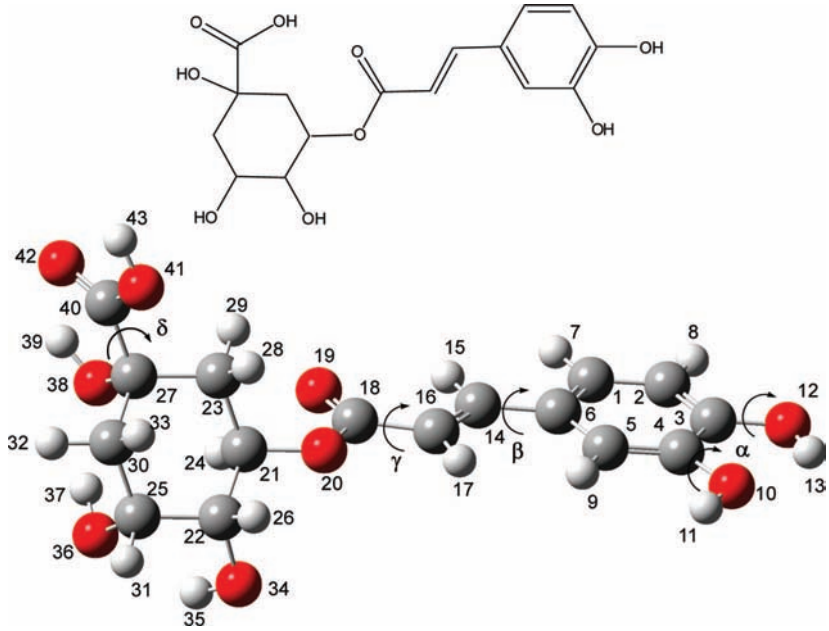

Figure 1. Chemical structure and geometry of chlorogenic acid with the atomic numbering used in the text.

2. Experimental and Theoretical Methods

2.1. Reagents and Chemicals. Chlorogenic acid was obtained from Sigma. Pb^{2+} stock solutions were prepared from lead chloride. Water was delivered by a Milli-Q-water purification system. The stoichiometry of the complexes was determined by the molar ratio method from the UV−visible data set. For this method, solutions containing a constant concentration (6×10^{-5} M) of chlorogenic acid in water and variable concentration of Pb^{2+} (from 6×10^{-6} to 1.5×10^{-4} M) were used. A broad range of metal-to-ligand molar ratios was used in the equilibrium studies. The pH was kept constant during the dosage (pH 6). Ionic strength was fixed to 0.1 M with NaCl.

2.2. Instrumentation. The UV−visible spectra were recorded on a Cary-l (Varian) spectrophotometer with cells of 1 cm path length, at 25 °C. A flow cell was used to allow successive additions of small amounts of lead chloride directly in the ligand solution

2.3. Chemometric methods. The absorption spectra collected during the course of the metal-binding experiment were analyzed with the fitting program SPECFIT (version 3.0).[36] This software allows the determination of the number of species that contribute to the absorption spectra, using a factor analysis procedure (EFA),[37−39] and of the electronic spectrum of each pure species. The Specfit software has also been used to estimate the apparent stability constants (β) of the different complexed forms. To obtain the best fit between the complexation model and the experimental data, several models of complexes have been envisaged for the refinement of the stability constants. The apparent stability constant

$$\beta = [Pb_aL_b]/[Pb]^a \cdot [L]^b$$

results from the equilibrium between the free ligand L and the complex Pb_aL_b (without taking into account the protonation state of the ligand):

$$a\mathrm{Pb(II)} + b\mathrm{L} \leftrightarrow \mathrm{Pb}_a\mathrm{L}_b$$

2.4. Quantum Chemical Calculations. All calculations were performed at the density functional level of theory with the B3LYP hybrid functional,[40,41] using the Gaussian (G03) program package.[42] Geometry optimizations were carried out without any symmetry constraints. A double-ξ quality LANL2DZ effective core potential[43] was used for the lead atom and the 6-31+G(d,p) basis set, including polarization functions to improve the description of intramolecular H-bonding in the ligand, for the other atoms. Vibrational frequency calculations have been performed to ensure that all the optimized structures of free and complexed ligands correspond to energy minima. The low-lying excited states were treated within the adiabatic approximation of time-dependent density functional theory (DFT-RPA)[44] with the B3LYP hybrid functional. Vertical excitation energies were computed for the first 40 singlet excited states, in order to reproduce the UV−visible spectra of free and complexed ligands. As it is well-known that the UV−visible absorption spectra are very sensitive to the solvent effects, these latter were introduced by the SCRF method, via the Polarized Continuum Model (IEF-PCM)[45,46] implemented in the Gaussian program.

3. Results and Discussion

3.1. Structure of Chlorogenic Acid and Its Deprotonated Derivatives. The necessary first step of this work was the determination of the most stable conformation of H_3CGA. Indeed, this molecule is very flexible, with several rotational degrees of freedom that must be explored to ensure its geometry. Furthermore, the presence of a six-membered ring induces taking into account both its chair and boat conformations. The dihedral angles manipulated to investigate all the possible forms are indicated in Figure 1. α controls the orientation of the hydroxyl groups of the catechol moiety. Only one dihedral angle is needed (to rotate simultaneously both OH groups) because of the stabilizing effect of the presence of a hydrogen bond (O10H13). The β angle monitors the orientation of the benzene ring with respect to the chain and consequently the electronic delocalization between these two entities, depending on their planarity. The variation of the γ angle allows forming a cis or a trans conformer and δ accounts for the rotation of the carboxylic function bonded to the six-membered ring. The conformation reported in Figure 1 will be taken as reference, in which all the dihedral angles have the value 0.

To determine the most stable geometry of chlorogenic acid, 32 structures were optimized. The starting point of each

TABLE 1: Main Dihedral Angles Calculated for the 16 Most Stable Conformers of H_3CGA with Their ZPVE Energy[a]

	α	β	γ	δ	energy (hartrees)	ΔE (kcal·mol^{-1})
1	1.5	0.7	0.5	3.3	−1297.257314	0
2	0.0	177.8	1.9	4.4	−1297.256923	0.2
3	179.6	0.7	0.1	3.9	−1297.256557	0.5
4	179.9	175.1	2.0	5.1	−1297.256053	0.8
5	0.8	0.1	175.2	2.7	−1297.255882	0.9
6	2.1	176.6	172.5	1.2	−1297.255387	1.2
7	179.8	3.4	173.3	2.3	−1297.255055	1.4
8	179.5	178.6	176.7	3.3	−1297.254744	1.6
9	0.8	176.5	3.5	159.7	−1297.253206	2.6
10	1.2	1.3	1.5	162.3	−1297.253188	2.6
11	179.8	2.7	2.5	159.8	−1297.252927	2.8
12	1.4	177.3	173.1	150.8	−1297.252904	2.8
13	179.8	175.7	2.0	163.7	−1297.252068	3.3
14	0.7	1.7	177.9	165.7	−1297.251751	3.5
15	179.9	2.4	174.1	163.9	−1297.250957	4.0
16	179.7	179.5	176.3	163.1	−1297.250616	4.2

[a] ΔE is the relative energy with respect to the most stable one (conformer **1**).

optimization corresponds to a set of values of the previously defined dihedral angles, associated to either the chair or the boat conformation of the six-membered ring. A systematic approach was taken to generate these initial structures: the dihedral angles were set to 180° one by one, then two by two, and so on. All the combinations are reported in Table 1 for the chair conformer. The corresponding optimized conformers are labeled **1** to **16** in the order of increasing energy. It can be seen in Table 1 that the lowest energy is associated with the conformer in which all the angles are close to 0, i.e., the geometry depicted in Figure 1. When only one angle is modified, the energy does not vary very much except for δ. The rotation of the carboxylic group is very destabilizing, and the 8 conformers in which it occurs have the highest energy. This is probably due to the presence of the H39O42 H-bond that is broken when the rotation is performed. The cis or trans conformation of the chain also has a great importance. Indeed, the 4 conformers with lowest energy have $\gamma \approx 0$, showing that the trans isomers are preferred. The same calculations have been performed with a boat six-membered ring, but results are not presented here because all the energies are higher than those obtained for the chair form. A recent paper reports the structure of H_3CGA optimized at the B3LYP/6-31G(d) level of theory, but the reported conformation is not the most stable.[47] This conformation corresponds to conformer **8** found in this study.

The optimized geometry of the most stable conformer **1** (Figure 1) is reported in Tables 2 and 3. It is characterized by the coplanarity of the benzene ring and the chain. It is interesting to note that the geometrical parameters of both these moieties are quasi-identical as in caffeic acid (*trans*-3-(3,4-dihydroxyphenyl)propenoic acid).[48] Indeed all the bond lengths are strictly identical in both compounds as well as the angles with, however, two exceptions: the C16C18O20 and C16C18O19 angles that increase by 1.1 and 0.5°, respectively, in chlorogenic acid with respect to caffeic acid. These very small variations show that the substitution of a hydrogen atom by the substituted six-membered ring present in chlorogenic acid has quasi-no effect on the structural properties of this moiety. In the saturated ring, all the CC bonds have similar lengths with a maximum difference of 0.012 Å. The CO bond lengths of the cyclohexane ring considerably differ (1.413 to 1.430 Å) according to the formation of intramolecular H-bond with their H atom. Indeed, C22O34 is the shortest one because H35 is not involved in the H-bond; the two other ones present a similar longer length and their hydrogen atoms form H-bonds of comparable strength.

TABLE 2: Bond lengths (Å) of Chlorogenic Acid and Its Deprotonated Forms

	H_3CGA	H_2CGA^-	$HCGA^{2-}$	CGA^{3-}
C1C2	1.393	1.396	1.384	1.379
C2C3	1.392	1.392	1.445	1.451
C3C4	1.411	1.407	1.465	1.525
C4C5	1.383	1.386	1.376	1.418
C5C6	1.412	1.411	1.428	1.435
C6C1	1.405	1.406	1.417	1.433
C6C14	1.457	1.464	1.434	1.416
C14C16	1.347	1.345	1.369	1.403
C16C18	1.472	1.485	1.455	1.417
C18O20	1.361	1.346	1.377	1.401
O20C21	1.442	1.461	1.445	1.446
C21C22	1.535	1.535	1.535	1.542
C22C25	1.546	1.543	1.539	1.549
C25C30	1.534	1.530	1.540	1.535
C30C27	1.546	1.539	1.530	1.543
C27C23	1.542	1.539	1.542	1.540
C23C21	1.534	1.529	1.538	1.540
C27C40	1.527	1.575	1.575	1.577
C3O12	1.357	1.367	1.264	1.264
C4O10	1.376	1.382	1.387	1.279
C18O19	1.218	1.220	1.229	1.259
C22O34	1.413	1.426	1.427	1.416
C25O36	1.429	1.437	1.439	1.433
C27O38	1.430	1.442	1.445	1.447
C40O41	1.342	1.248	1.249	1.250
C40O42	1.215	1.269	1.271	1.275
O12H13	0.970	0.969		
O10H11	0.965	0.966	0.966	
O41H43	0.973			
O10--H13	2.113	2.147		
H37--O38	1.916	1.865	1.861	1.874
H39--O42	2.002	1.731	1.736	1.738
O42--H43	2.000			
O19--H35				1.709

Upon deprotonation of the carboxylic function to give H_2CGA^-, the aromatic ring remains unchanged, contrary to the carbon chain (Tables 2 and 3). Indeed, the three bonds linking C16 to C21 alternatively increase and decrease reflecting a more localized character of the electronic distribution. The CC bonds of the saturated ring exhibit only minor modifications, whereas the substituents are much more affected. As expected, the carboxylate group presents an electronic delocalization between its two CO bonds with an opening of the OCO angle, accompanied by a shortening of the C27C40 bond length. All the CO bonds of the hydroxyl functions increase and the H39--O42 hydrogen bond shows an important reinforcement. Concerning the relative position of the different moieties of the anion, it can be seen that cyclohexane is rotated by ∼36° with respect to the chain compared to its position in the neutral compound.

For the bideprotonated form, $HCGA^{2-}$, two possibilities must be envisaged for the departure of the second hydrogen: H11 or H13 of the catechol group. It will be exhibited later that the second deprotonation occurs at the O12H13 hydroxyl. The geometrical parameters of $HCGA^{2-}$ are reported in Tables 2 and 3. The major changes with respect to the previous compounds concern the electronic distribution in the phenyl ring and the carbonated chain. Indeed, the ring acquires a quinoidal conformation with a decrease of C1C2 and C4C5 bond lengths associated to an increase of the four others. This is accompanied by a modification of the electronic distribution of the substituents to preserve the conjugation: a great shortening of C3O12 bond

TABLE 3: Valence and Main Dihedral Angles (deg) of Chlorogenic Acid and Its Deprotonated Forms

	H_3CGA	H_2CGA^-	$HCGA^{2-}$	CGA^{3-}
C1C2C3	119.9	120.0	123.2	123.3
C2C3C4	119.3	119.1	113.3	117.0
C3C4C5	120.8	120.9	122.8	116.1
C4C5C6	120.5	120.6	122.4	125.1
C5C6C1	118.1	117.8	116.1	117.2
C6C1C2	121.5	121.5	122.3	121.3
C1C6C14	118.9	119.3	120.0	116.3
C6C14C16	128.2	127.6	129.6	130.5
C14C16C18	120.1	121.0	121.2	121.4
C16C18O20	110.4	109.7	110.7	113.3
C18O20C21	116.9	119.6	119.0	118.8
O20C21C22	106.7	107.1	108.3	112.1
C21C22C25	111.5	111.2	111.6	111.5
C22C25C30	112.6	111.7	111.6	110.3
C25C30C27	111.1	111.7	111.8	111.7
C30C27C23	110.1	109.7	109.7	109.7
C27C23C21	110.6	111.2	112.2	113.6
C23C21C22	112.8	112.6	111.8	110.7
C3C4O10	114.4	114.9	115.7	119.6
C4C3O12	120.3	120.6	122.7	122.2
C16C18O19	126.1	124.6	126.8	127.9
C21C22O34	111.6	111.6	112.3	114.1
C22C25O36	109.2	108.9	109.6	113.5
C30C27O38	109.2	108.9	108.8	109.1
C30C27C40	110.3	110.7	110.2	109.8
C27C40O41	113.8	117.1	117.5	118.0
C27C40O42	122.6	112.8	113.2	113.5
C2C1C6C14	179.5	179.9	179.7	179.6
C1C6C14C16	179.7	179.4	179.7	179.6
C6C14C16C18	178.9	179.5	179.3	179.1
C14C16C18O19	0.4	0.6	0.4	2.9
C14C16C18O20	179.5	179	179.9	176.0
C16C18O20C21	175.6	176.6	176.6	164.9
C18O20C21C22	149.2	113.7	111.1	85.8
C18O20C21C23	88.5	124.6	127.4	153.5
C23C27C40O42	122.0	120.8	120.3	120.2

length that acquires a double character, and alternative decrease and increase of the bond lengths of the chain, beginning by the shortening of C6C14. The rest of the molecule is only slightly affected by the second deprotonation.

And finally, the structure of the trideprotonated chlorogenic acid, CGA^{3-}, with the departure of H11, has been inspected. In this species, all the bonds of the phenyl ring lengthen except C1C2 which decreases, compared to $HCGA^{2-}$. The formation of two CO double bonds in place of the hydroxyl groups induces a strong increase of C3C4 that acquires a single character. Concerning the chain, a reinforcement of the previous trend is observed with a decrease of C6C14 and alternative increase and decrease of the following bond lengths. And once more, the cyclohexane part of the molecule is only slightly affected by deprotonation. The major change is the rotation of this ring with respect to the chain of about 25°.

3.2. Electronic Spectroscopy of Chlorogenic Acid and Its Derivatives. Figure 2 shows the absorption electronic spectra of chlorogenic acid in aqueous solution at different pH (from 2 to 12). In very acidic conditions, H_3CGA presents a double absorption band at 324 and 295 nm. By increasing the pH to ~5 the general shape of the spectrum is quasi-unmodified, then for higher pH, a new band appears at 371 nm. An isosbestic point is observed at 341 nm until pH 10. For higher pH values, an important decrease of the absorption is observed. The set of spectra treated by evolving factor analysis (EFA) has allowed the determination of the pure UV−visible spectrum of each form of chlorogenic acid. The two first forms, fully protonated and

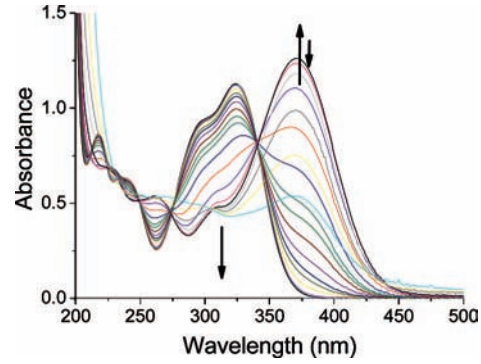

Figure 2. Evolution of the chlorogenic acid absorption spectrum with the pH in the range 2−12. $[H_3CGA] = 6 \times 10^{-5}$ M.

TABLE 4: Comparison of the pK_a Values Obtained in This Study with Those Reported in the Literature (with the references)

	this work	lit.
pK_a(COOH)	3.52	3.36[29]
		3.35[49]
		3.35[50]
		3.37[51]
pK_a(OH1)	8.68	8.25[29]
		8.21[49]
		8.30[50]
		8.27[51]
pK_a(OH2)	11.8	12.3[29]
		12.5[49]
		11.5[50]
		12.1[51]

monodeprotonated, have exactly the same absorption profile. The bideprotonated form is characterized by the absorption at 371 nm, whereas the spectrum of the trideprotonated form is less well defined (bad fit), which can be explained by a degradation of the molecule occurring for high pH. From the data set, the acidity constants were calculated and refined with the Specfit program. The estimated values of the dissociation constants are shown in Table 4, along with the values obtained by potentiometric titrations reported in the literature,[29,49−51] and a good agreement is found. The results collected in literature seem to confirm that the CGA^{3-} species is more difficult to characterize insofar as the set of pK_a values is less homogeneous than for the other species.

For each of the previously studied derivatives of chlorogenic acid, the electronic transitions have been calculated by time-dependent DFT, taking into account the solvent effects. The UV−vis spectrum of H_3CGA (Figure 3) is characterized by four absorption bands in the 200−400 nm spectral range. The calculated spectrum of conformer **1** is in very good agreement with the experimental one as shown in Figure 3a and Table 5. The longest wavelength transition largely corresponding to the HOMO → LUMO transition (H → L) presents mainly a $\pi\pi^*$ character with an electronic density localization on the benzene ring and the carbon chain (Figure 4), as well as the transition calculated at 289 nm (H − 1→ L). The two other transitions, calculated at 239 and 217 nm, also present the same $\pi\pi^*$ character with the same electronic localization, showing that only one part of the molecule is responsible for the observed transitions. It can be seen that the L + 1 MO, involving the carboxylic function, does not participate to the calculated transitions. The electronic transitions have also been calculated for the more stable isomers **2**, **3**, and **4.** The calculated wavelengths are reported in the Table 6 and compared to the

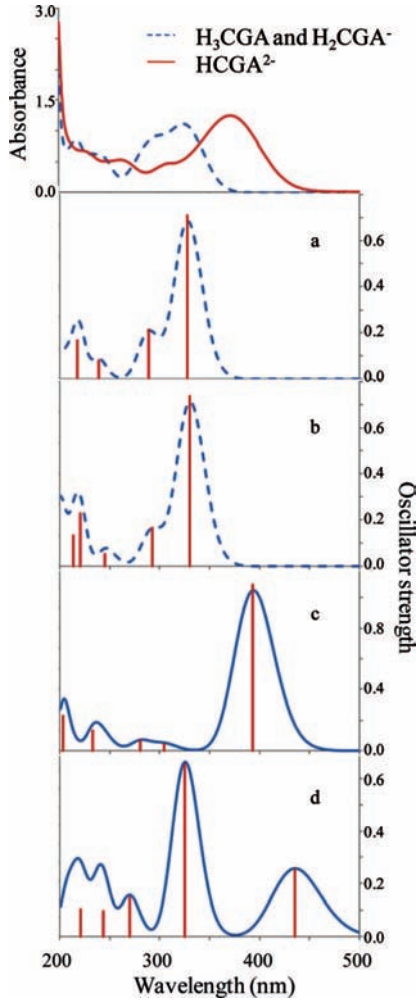

Figure 3. Absorption spectrum of H_3CGA, H_2CGA^-, and $HCGA^{2-}$ obtained by numerical treatment of the data set and theoretical spectrum of H_3CGA (a), H_2CGA^- (b), $HCGA^{2-}$ with a deprotonation of the O12H13 hydroxyl, (c) and $HCGA^{2-}$ with a deprotonation of the O10H11 hydroxyl (d). The theoretical spectra have been plotted by considering a constant fwhm of 3000 cm^{-1}.

experimental ones. It can be seen that conformers **1** and **3** present very close theoretical electronic spectra. In a same way, the theoretical spectra of conformers **2** and **4** are quasi-identical. In these two pairs, only the orientation of the hydroxyl functions of the catechol moiety differs, revealing that this orientation has very little influence on the calculated electronic transition positions. In opposition, the calculated wavelength difference between these two pairs is more important, showing the greater impact of the rotation of the benzene ring with respect to the carbonated chain. Although the differences are not so important, the spectra of conformers **2** and **4** are in worse agreement with the experimental data than that of conformer **1**.

The H_2CGA^- absorption spectrum extracted by chemometric methods is identical to that of the neutral species (Figure 3). From a theoretical point of view, some little differences exist but the agreement with experiment remains very satisfying (Table 5). The H → L transition, calculated at 330 nm, involves MOs that have the same shape as those of H_3CGA (Figure 4). The H − 2 MO has the same electronic localization as H − 1 in H_3CGA, so the transitions calculated at 289 and 293 nm in H_3CGA and H_2CGA^-, respectively, are equivalent. In the same way, L + 1 and H − 8 for H_2CGA^- correspond to L + 2 and H − 5 for H_3CGA, respectively. So, the absorption bands observed at 236 and 214 nm for both compounds are associated

TABLE 5: Experimental and Calculated Absorption Wavelengths (in water) of H_3CGA, H_2CGA^-, and $HCGA^{2-}$ and MO's (with monoexcitation) Contributions Involved in Each Transition[a]

H_3CGA				H_2CGA^-				$HCGA^{2-}$							
								spectrum c				spectrum d			
λ_{exp} (nm)	λ_{calc} (nm)	f	MO contribution (%)	λ_{exp} (nm)	λ_{calc} (nm)	f	MO contribution (%)	λ_{exp} (nm)	λ_{calc} (nm)	f	MO contribution (%)	λ_{calc} (nm)	f	MO contribution (%)	
324	328	0.71	H → L (79)	324	330	0.74	H → L (81)	371	393	1	H → L (76)	435	0.25	H → L (76)	
395	289	0.21	H − 1 → L (82)	295	293	0.17	H − 2 → L (79)	307	304	0.05	H − 1 → L (85)	325	0.65	H − 1 → L (85)	
236	239	0.08	H → L + 2 (64), H − 5 → L (10)	236	245	0.05	H → L + 1 (44), H − 5 → L (35)	261	280	0.07	H → L + 2 (78)	270	0.15	H → L + 2 (78)	
217	217	0.17	H − 5 → L (47), H − 6 → L (26)	217	220	0.23	H − 8 → L (74)	227	233	0.13	H − 6 → L (60), H → L + 8 (12)	243	0.10	H − 6 → L (60), H → L + 8 (12)	
					214	0.13	H → L + 4 (54), H − 2 → L + 1 (33)		203	0.23	H − 1 → L + 2 (46), H − 1 → L + 8 (10)	220	0.10	H − 1 → L + 2 (46), H − 1 → L + 8 (10)	

[a] f is relative to the oscillator strength. The spectra c and d are relative to the Figure 4.

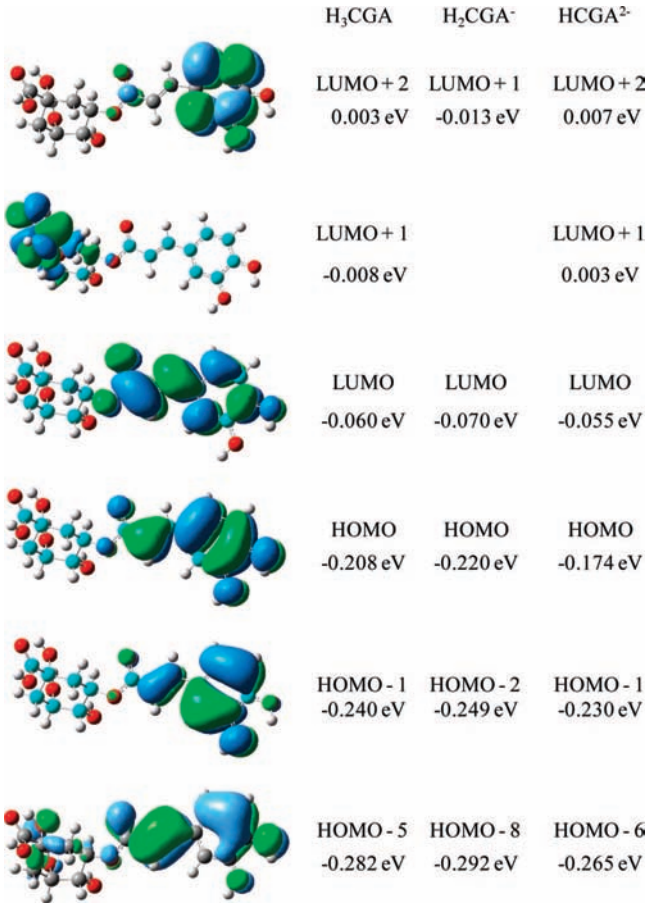

Figure 4. Molecular orbitals involved in the calculated transitions of H_3CGA, H_2CGA^-, and $HCGA^{2-}$, with their energies.

TABLE 6: Experimental Absorption Wavelengths of H_3CGA and Electronic Transitions Calculated from the Optimized Structures of Conformers 1 to 4

	λ_{calc} (nm)			
λ_{exp} (nm)	**1**	**2**	**3**	**4**
324	328	334	329	336
395	289	287	291	288
236	239	239	238	239
217	217	206	216	206

to the same calculated transitions. Furthermore, it can be noted that H − 1 of H_2CGA^-, which is a nonbonding orbital (not shown) localized on the carboxylate group, is not involved in the calculated electronic transitions.

For the bideprotonated species $HCGA^{2-}$, two cases must be envisaged according to the hydroxyl function that loses its hydrogen: O12H13 or O10H11. The corresponding electronic spectra have been calculated (Figure 3 and Table 5) and, by comparison with experimental spectrum, it is obvious that deprotonation occurs at the O12H13 hydroxyl. The experimental absorption spectrum is characterized by an intense band at 371 nm and three others of lower intensity in the short wavelength range. This is well reproduced by calculations that give an intense transition at 393 nm and the others with smaller oscillator strengths. Even if the calculated wavelengths are not in perfect agreement with the experimental ones (as expected for calculations on negatively charged species) an unambiguous assignment of the observed bands can be realized. The long wavelength transition (H → L) involves MOs with the same shape of the corresponding ones in H_3CGA. In fact, all transitions in

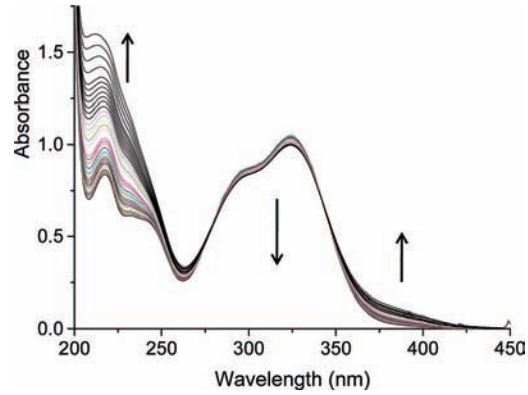

Figure 5. UV−vis spectra of chlorogenic acid at pH 6, in the absence and the presence of $PbCl_2$ for metal/ligand ratios varying from 0 to 3.

$HCGA^{2-}$ are strictly comparable to that of H_3CGA as H − 1, H, L, and L + 2 MOs are the same in both compounds, and H − 5 of H_3CGA is equivalent to H − 6 of $HCGA^{2-}$. It should be noted that the spectra of the three studied species are due to the same transitions that are only shifted for the bideprotonated form.

3.3. Complexation of Pb(II) by Chlorogenic Acid. The dosage of the complexation reaction of Pb(II) by chlorogenic acid, in aqueous solution at pH 6, has been followed by UV−vis spectroscopy, for [Pb(II)]/[H_2CGA^-] molar ratios from 0 to 3 (Figure 5). At this pH, only the H_2CGA^- species is initially present in the solution. The lead(II) complexation induces only a few spectral modifications. The characteristic absorption band of H_2CGA^-, localized at 324 nm, is not very affected by the metal salt addition, and the main modifications are observed in the low wavelengths range where an important increase in the absorbance is observed around 225 nm. A new band, of low intensity, appears with a wavelength slightly lower than 400 nm. Using the molar ratio method, the curves of absorbance variations versus [Pb(II)]/[H_2CGA^-] molar ratio plotted at different wavelengths (214 and 380 nm) allow the observation of two complexed forms of stoichiometry (metal:ligand) 1:1 and 2:1 (results not shown). From the UV−vis spectra set, the determination of the number of different absorbing species was estimated by the EFA method. With this method, four absorption spectra corresponding to pure species have been determined. The characteristic spectra obtained with the chemometric methods of H_2CGA^-, 1:1 complex, 2:1 complex, and free Pb(II) are represented in Figure 6a. The 1:1 complex spectrum is perfectly identical with that of H_2CGA^-. The free Pb(II) in solution presents a low absorbance under 270 nm that has been taken into account in the numerical treatment. The calculated values of the stability constants, fitted from experimental data, of the two complexes are respectively $\log \beta_{1:1} = 3.39 \pm 0.21$ and $\log \beta_{2:1} = 7.12 \pm 0.09$. The concentration variations of the different species versus the quantity of Pb(II) added are plotted in Figure 6b. The 1:1 complex, where only one complexing site is implied, is formed at the beginning of the metal addition. However, the formation of the 2:1 complex, where a second metal fixing site is involved, starts for a molar ratio of 0.1. This observation tends to show that the two sites in competition for the metal fixing have relatively close complexing capacities. The curves of the concentration evolution of the various species reveal that the formation of complex remains weak, even with a molar ratio of 3. For a molar ratio of 1, scarcely 15% of the chlorogenic acid is complexed, whereas studies carried out with Al(III) show that with this same ratio, more than 60% of the

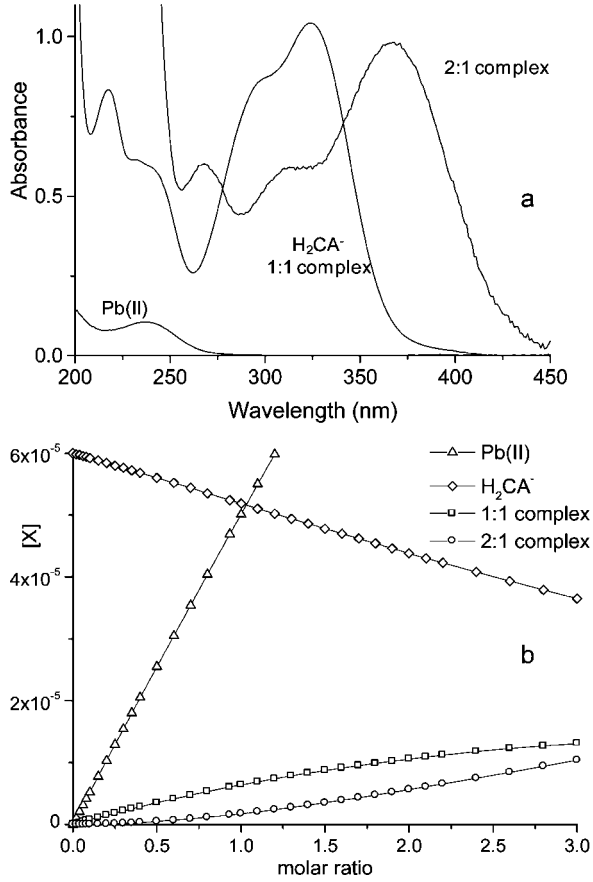

Figure 6. UV−vis spectra of the free ligand, 1:1 and 2:1 complexes obtained by numerical treatment of the data set (a) and distribution curves of the concentration of the different species in solution as a function of [Pb(II)]/[H_2CGA^-] molar ratio.

ligand is complexed (results not published). For the purpose of comparison, in the same medium, caffeic acid, which involves the same complexing sites in competition, forms complexes of the same stoichiometry, with stability constants of log $\beta_{1:1}$ = 5.77 and log $\beta_{2:1}$ = 10.8.[33] Thus, H_2CGA^- presents a complexing power clearly lower than that of the caffeate ion.

To determine the preferential complexing site of Pb(II), in other words, the site involved in the 1:1 complex, the theoretical spectra have been calculated from different possible complexed forms. In all cases, the structure of these forms has been optimized and solvent effects have been taken into account in the TD-DFT calculations. Our previous works[33,35] suggest that in such experimental conditions (water solution, pH ∼6), the Pb ion has a pentacoordinated environment. So, in all the calculations, water molecules have been added to Pb(II) to reach a coordination number of 5. Even if the most probable sites of metal fixing are the carboxylate and catechol functions, the other functions such as the carbonyl C18O19 were tested. In the same way, the two fixing modes mono- and bidentate were considered. For the sake of clarity, only the three theoretical spectra nearest the experimental spectrum of the 1:1 complex were reported in Figure 7. In this figure, the theoretical spectra correspond to complexes involving the carboxylate group in bidentate and monodentate mode $[Pb(H_2CGA)(H_2O)_3]^+_{bi}$ and $[Pb(H_2CGA)(H_2O)_4]^+_{mono}$, respectively, and to a complex obtained by metal chelation via the catecholate group $[Pb(CGA)(H_2O)_3]^-_{bi}$. The calculated wavelengths are reported in Table 7. The electronic transition, mainly implicating H → L, calculated in the long wavelengths range allows the identification of the complex structure. Indeed, the wavelength calculated at 333 nm for

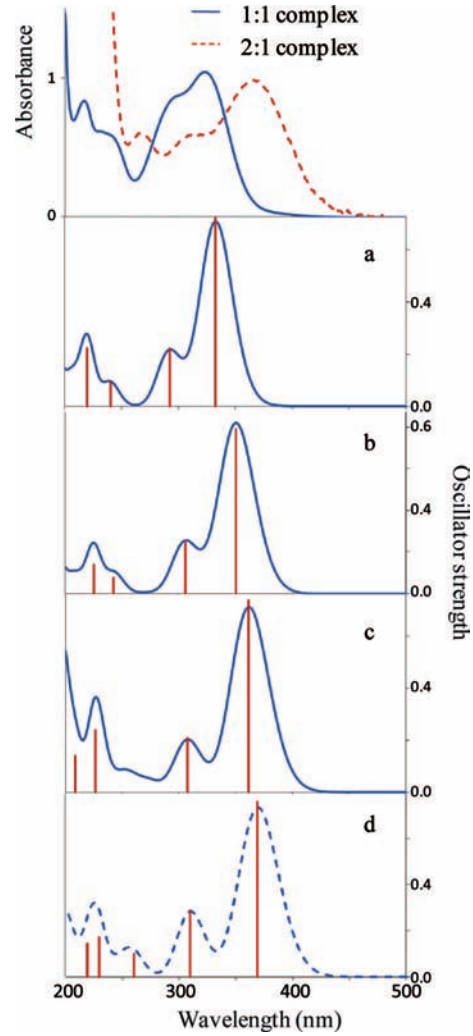

Figure 7. Absorption spectrum of 1:1 and 2:1 complexes obtained by numerical treatment of the data set and theoretical spectrum of $[Pb(H_2CGA)(H_2O)_3]^+_{bi}$ (a), $[Pb(H_2CGA)(H_2O)_4]^+_{mono}$ (b), $[Pb(CGA)(H_2O)_3]^-_{bi}$ (c), and $[Pb_2(CGA)(H_2O)_6]^+$ (d). The theoretical spectra have been plotted by considering a constant fwhm of 3000 cm^{-1}.

$[Pb(H_2CGA)(H_2O)_3]^+_{bi}$ (Figure 7a) is in good agreement with the experiment (324 nm), with the same error range as the value calculated for the monodeprotonated ligand. For $[Pb(H_2CGA)(H_2O)_4]^+_{mono}$ (Figure 7b) and $[Pb(CGA)(H_2O)_3]^-_{bi}$ (Figure 7c) the difference between theoretical and experimental values is much more pronounced: 26 and 38 nm, respectively. So what makes it possible to exclude these two structures. So, the Pb(II) ion is preferentially coordinated to the carboxylate function to form a chelate. In this complex, all the MO involved in the different electronic transitions have exactly the same shape as those involved in the transitions calculated for H_2CGA^- (Figure 8). So neither ligand-to-metal nor metal-to-ligand charge transfer is observed in the 1:1 complex spectrum; the electronic density is always localized on the benzene ring and carbon chain of the ligand. The electronic density is localized on the metal ion for the L + 1 and L + 2 MOs, but these orbitals are never involved, even with a low contribution, in the calculated transitions with non-negligible oscillator strength. In opposition, in $[Pb(H_2CGA)(H_2O)_4]^+_{mono}$, these two MO are identical with those of $[Pb(H_2CGA)(H_2O)_3]^+_{bi}$, but they participate with a minor contribution (15−20%) to the calculated transitions. This fact could explain the difference in the calculated spectra of $[Pb(H_2CGA)(H_2O)_3]^+_{bi}$ and $[Pb(H_2CGA)(H_2O)_4]^+_{mono}$. Finally, in the three 1:1 complexed forms reported in Figure 7, the H

TABLE 7: Experimental and Calculated Absorption Wavelengths (in water) of the Complexes 1:1 and 2:1 and MO's (with Monoexcitation) Contributions Involved in Each Transition[a]

1:1 complex									2:1 complex		
		$[Pb(H_2CGA)(H_2O)_3]_{bi}^+$			$[Pb(H_2CGA)(H_2O)_4]_{mono}^+$		$[Pb(CGA)(H_2O)_3]_{bi}^-$			$[Pb_2(CGA)(H_2O)_6]^+$	
λ_{exp} (nm)	λ_{calc} (nm)	f	MO contribution (%)	λ_{calc} (nm)	f	λ_{calc} (nm)	f	λ_{exp} (nm)	λ_{calc} (nm)	f	MO contribution (%)
324	333	0.73	H → L (79)	350	0.79	362	0.74	367	369	0.76	H → L (80)
295	292	0.22	H − 1 → L (83)	305	0.24	308	0.21	311	310	0.29	H − 1 → L (84)
236	240	0.09	H → L + 3 (66), H − 5 → L (13)	242	0.08	227	0.24	267	260	0.10	H → L + 4 (86)
217	220	0.22	H − 5 → L (63)	225	0.14	209	0.14		229	0.17	H − 4 → L (53), H − 5 → L (31)
									219	0.14	H → L + 8 (46), H − 1 → L + 4 (31)

[a] f is relative to the oscillator strength.

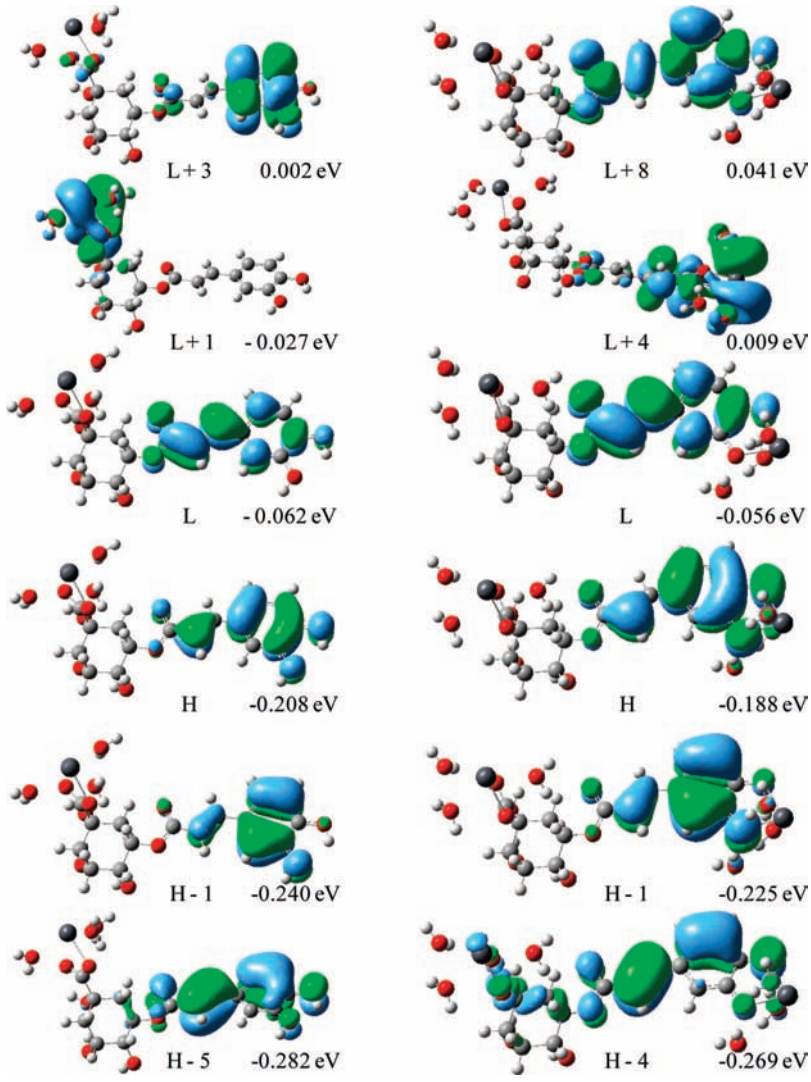

Figure 8. Molecular orbitals involved in the calculated transitions of $[Pb(H_2CGA)(H_2O)_3]^+_{bi}$ and $[Pb_2(CGA)(H_2O)_6]^+$, with their energies.

→ L transitions involve MOs having the same shape, but that differ in energy giving rise to very different absorption wavelengths.

Even if the carboxylate site is the first to be involved in the complexation of Pb(II), the catechol moiety rapidly takes part in the metal fixation with the formation of the 2:1 complex. The electronic spectrum of $[Pb_2(CGA)(H_2O)_6]^+$ has been calculated from its optimized structure and is reported in Figure 7d. This theoretical spectrum is in very good agreement with the experimental spectrum of 2:1 complex (Table 7). $[Pb_2(CGA)(H_2O)_6]^+$ has been obtained by Pb(II) chelation with both carboxylate and fully deprotonated catechol groups. Once more, the two transitions calculated in the long wavelength range, H → L and H − 1 → L, computed at 369 (exptl 367 nm) and 310 nm (exptl 311 nm), respectively (Figure 8), involve MOs with the same shape as those calculated for the different

TABLE 8: Structural Parameters of $[Pb(H_2CGA)(H_2O)_3]_{bi}^+$ and $[Pb_2(CGA)(H_2O)_6]^+$Bond Lengths (Å), Valence Angles (deg), and Main Dihedral Angles (deg)

valence angles			dihedral angles		
	1:1	2:1		1:1	2:1
C1C2	1.392	1.39	C1C2C3	119.9	120.5
C2C3	1.393	1.404	C2C3C4	119.4	118.8
C3C4	1.414	1.433	C3C4C5	120.7	120.0
C4C5	1.382	1.387	C4C5C6	120.4	121.1
C5C6	1.414	1.416	C5C6C1	118.2	118.2
C6C1	1.406	1.409	C6C1C2	121.4	121.4
C6C14	1.453	1.447	C1C6C14	118.8	118.7
C14C16	1.351	1.356	C6C14C16	128.3	128.4
C16C18	1.465	1.457	C14C16C18	120.0	120.2
C18O20	1.368	1.375	C16C18O20	110.7	110.9
O20C21	1.435	1.429	C18O20C21	116.7	115.8
C21C22	1.537	1.535	O20C21C22	106.7	180.1
C22C25	1.547	1.548	C21C22C25	111.5	110.9
C25C30	1.538	1.537	C22C25C30	112.9	113.3
C30C27	1.548	1.540	C25C30C27	110.9	111.8
C27C23	1.539	1.545	C30C27C23	110.2	110.1
C23C21	1.535	1.538	C27C23C21	111.2	110.7
C27C40	1.522	1.526	C23C21C22	112.0	111.5
C3O12	1.352	1.335	C3C4O10	114.2	118.2
C4O10	1.372	1.365	C4C3O12	120.3	119.3
C18O19	1.222	1.224	C16C18O19	126.7	127.4
C22O34	1.407	1.407	C21C22O34	112.0	111.9
C25O36	1.426	1.426	C22C25O36	109.6	109.4
C27O38	1.431	1.426	C30C27O38	110.7	106.8
C40O41	1.279	1.277	C30C27C40	110.1	111.4
C40O42	1.274	1.280	C27C40O41	121.3	121.0
O12H13	0.970		C27C40O42	119.8	120.3
O10H11	0.965		C40O41Pb	95.0	91.6
O41H43			C40O42Pb	89.2	92.8
O10--H13	2.115		C3O12Pb		113.3
H37--O38	1.985	1.996	C4O10Pb		110.5
H39--O42	2.153	2.616	C2C1C6C14	179.6	179.3
O41Pb	2.256	2.317	C1C6C14C16	176.0	179.4
O42Pb	2.387	2.288	C6C14C16C18	179.0	178.2
O10Pb		2.193	C14C16C18O19	0.9	0.8
O12Pb		2.124	C14C16C18O20	178.7	179.4
			C16C18O20C21	173.6	173.3
			C18O20C21C22	160.9	158.1
			C18O20C21C23	77.5	80.1
			C23C27C40O42	131.2	103.4
			C27C40O41Pb	171.6	176.1
			C3C4O10Pb		3.2

protonation states of chlorogenic acid. For this complexed form, the two long wavelength bands red shift with respect to the free ligand or 1:1 complex and a new band appears at 267 nm. This band is characterized by a low ligand−metal charge transfer, with a displacement of the charge density from the carbon chain to the Pb atom bound to the catechol (H → L + 4 transition).

3.4. Complexe Structures. Only the structures of the two identified complexes $[Pb(H_2CGA)(H_2O)_3]^+_{bi}$ and $[Pb_2(CGA)(H_2O)_6]^+$ are reported in Table 8. Even if the Pb(II) coordination occurs at the level of the carboxylate group in the 1:1 complex, a low electronic effect is observed on the conjugated part of the ligand. Indeed, a low quinoidal form is adopted by the benzene ring, inducing noticeable variations in the CC and CO bond lengths in the carbon chain. At the level of the cyclohexane ring, the main modifications consist of a strengthening of all the CO bonds of the hydroxyl functions, and a rotation of 47° of this ring around the O20C21 bond is calculated. The two CO bonds of the carboxylate function acquire similar lengths in opposition to the free ligand H_2CGA^-. Moreover, the O41C40O42 valence angle significantly decreases (118.8°) with respect to the free ligand (130.1°) to form the chelate. Due to the presence of lone pair on the Pb atom, the ligands (H_2CGA^- and 3 water molecules) adopt a hemidirected arrangement[52,53] (as can be seen in Figure 8) that induces structural distortions. This leads to two PbO bond lengths with the carboxylate that differ by 0.13 Å. The PbO_{H_2O} bond lengths are longer with an average value of 2.505 Å.

As expected, for the structure of $[Pb_2(CGA)(H_2O)_6]^+$, the main changes with respect to $[Pb(H_2CGA)(H_2O)_3]^+_{bi}$ are localized at the catechol site level. An increase of the C2C3 and C3C4 bond lengths is achieved with a decrease of the C3O12 great dissymmetry is observed in the second chelate, in which the two CO and PbO bonds differ of 0.03 and 0.07Å, respectively.

4. Conclusion

Interest for the mechanism of metal cation complexation has grown in recent years. One key aspect of this interest resides in the quest for a better understanding of the metal−ligand interactions in chemical, environmental, and biochemical processes. However, the majority of these interactions occur in aqueous medium with very weak metal ion concentrations and, consequently, their studies require very sensitive techniques of molecular investigation. The UV−visible absorption spectroscopy combined with chemometric methods makes it possible to easily obtain information concerning the complexation processes (stoichiometry, stability constants, spectrum of pure species) but gives no information of structural nature about the complexed species. In this paper, we show that, from the spectral shape obtained by electronic spectroscopy, it is possible with quantum chemical methods, and in particular TD-DFT methodology, to identify the structure of a complex. That requires considering all the possible interactions between the ligand and metal ion and comparing the theoretical spectra obtained starting from the hypothetical structures of the various complexes with the experimental spectrum.

This methodology was successfully applied in the case of the Pb(II) complexation by a multisite ligand: the chlorogenic acid, which is a precursor of humic substances. We have shown that the Pb cation forms a chelate with the carboxylate function of the ligand.

References and Notes

(1) Chlopecka, A. *Water, Air, Soil Pollut.* **1996**, *45*, 297.
(2) Xian, X. *Plant Soil* **1989**, *113*, 257.
(3) Kabata-Pendias, A.; Pendias, H. *Trace Elements in Soils and Plants*; CRC Press: Boca Raton, FL, 2001.
(4) Davies, B. E. *Applied Soil Trace Elements*; John Wiley & Sons: New York, 1980.
(5) Schnitzer, M.; Khan, S. U. *Humic Substances in the Environment*; Marcel Dekker: New York, 1972.
(6) Piccolo, A. *Adv. Agron.* **2002**, *75*, 57.
(7) Schnitzer, M.; Khan, S. U. *Developments in Soil Science*; Vol. 8, Soil Organic Matter; Elsevier: Amsterdam, The Netherlands, 1978.
(8) Tipping, E. *Cation binding by Humic Substances*, *1st* ed; Cambridge University Press; Cambridge, UK, 2002.
(9) Evanko, C. R.; Dzombak, D. A. *Environ. Sci. Technol.* **1998**, *32*, 2846.
(10) Evanko, C. R.; Dzombak, D. A. *J. Colloid Interface Sci.* **1999**, *214*, 189.
(11) Giannakopoulos, E.; Stathi, P.; Dimos, K.; Gournis, D.; Sanakis, Y.; Deligiannakis, Y. *Langmuir* **2006**, *22*, 6863.
(12) Cornard, J. P.; Dangleterre, L.; Lapouge, C. *J. Phys. Chem. A* **2005**, *109*, 10044.
(13) Zang, L. Y.; Cosma, G.; Gardner, H.; Castranova, V.; Vallyathan, V. *Mol. Cell. Biochem.* **2003**, *247*, 205.
(14) Sisti, M.; De Santi, M.; Fraternale, D.; Ninfali, P.; Scoccianti, V.; Brandi, G. *LWT−Food Sci.Technol.* **2008**, *41*, 946.
(15) Zheng, L.-F.; Dai, F.; Zhou, B.; Yang, L.; Liu, Z.-L. *Food Chem. Toxicol.* **2008**, *46*, 149.

(16) Ma, C.-M.; Kully, M.; Khan, J. K.; Hattori, M.; Daneshtalab, M. *Bioorg. Med. Chem.* **2007**, *15*, 6830.
(17) Leenheer, J. A.; Rostad, C. E.; Gates, P. M.; Furlong, E. T.; Ferrer, I. *Anal. Chem.* **2001**, *73*, 1461.
(18) Lamy, I.; Cromer, M.; Scharff, J. P. *Anal. Chim. Acta* **1988**, *212*, 105.
(19) Hanninen, K. I.; Klocking, R.; Helbig, B. *Sci. Total Environ.* **1987**, *62*, 201.
(20) Kloecking, R.; Helbig, B. *Z. Chem.* **1976**, *16*, 189.
(21) Mugo, S. M.; Bottaro, C. S. *Rapid Commun. Mass Spectrom.* **2007**, *21*, 219.
(22) Cappiello, A.; De Simoni, E.; Fiorucci, C.; Mangani, F.; Palma, P.; Trufelli, H.; Decesari, S.; Facchini, M. C.; Fuzzi, S. *Environ. Sci. Technol.* **2003**, *37*, 1229.
(23) Rothe, J.; Plaschke, M.; Denecke, M. A. *Radiochim. Acta* **2004**, *92*, 711.
(24) Améziane, J.; Aplincourt, M.; Dupont, L.; Heirman, F.; Pierrard, J. C. *Bull. Soc. Chim. Fr.* **1996**, *133*, 243.
(25) Andjelkovic, M.; Van Camp, J.; De Meulenaer, B.; Depaemelaere, G.; Socaciu, C.; Verloo, M.; Verhe, R. *Food Chem.* **2006**, *98*, 23.
(26) Mahal, H. S.; Kapoor, S.; Satpati, A. K.; Mukherjee, T. *J. Phys. Chem. B* **2005**, *109*, 24197.
(27) Lamy, I.; Seywert, M.; Cromer, M.; Scharff, J.-P. *Anal. Chim. Acta* **1985**, *176*, 201.
(28) Méndez, J.; Lojo, M. I. *Microchem. J.* **1968**, *13*, 232.
(29) Adams, M. L.; O'Sullivan, B.; Downard, A. J.; Powell, K. *J. Chem. Eng. Data* **2002**, *47*, 289.
(30) Deng, Z.; Coudray, C.; Gouzoux, L.; Mazur, A.; Rayssiguier, Y.; Pepin, D. *Biol Trace Elem. Res.* **2000**, *76*, 245.
(31) Nagata, T.; Hayatsu, M.; Kosuge, N. *Phytochemistry* **1992**, *31*, 1215.
(32) Jurd, L.; Asen, S. *Phytochemistry* **1966**, *5*, 1263.
(33) Boilet, L.; Cornard, J. P.; Lapouge, C. *J. Phys. Chem. A* **2005**, *109*, 1952.
(34) Cornard, J. P.; Merlin, J. C. *Polyhedron* **2002**, *21*, 2801.
(35) Cornard, J. P.; Lapouge, C. *Chem. Phys. Lett.* **2007**, *438*, 41.
(36) Specfit Global Analysis System, SSA, Marlborough, MA, USA.
(37) Gampp, H.; Maeder, M.; Meyer, C. J.; Zuberbühler, A. *Talanta* **1986**, *33*, 943.
(38) Gampp, H.; Maeder, M.; Zuberbühler, A. D. *Trends Anal. Chem.* **1988**, *7*, 111.
(39) Maeder, M.; Zuberbühler, A. D. *Anal. Chem.* **1990**, *62*, 2220.
(40) Becke, A. D. *J. Chem. Phys.* **1993**, *98*, 5648.
(41) Lee, C.; Yang, W.; Parr, R. G. *Phys. Rev. B* **1988**, *37*, 785.
(42) Frisch, M. J.; Trucks, G. W.; Schlegel, H. B.; Scuseria, G. E.; Robb, M. A.; Cheeseman, J. R.; Montgomery, J. A., Jr.; Vreven, T.; Kudin, K. N.; Burant, J. C.; Millam, J. M.; Iyengar, S. S.; Tomasi, J.; Barone, V.; Mennucci, B.; Cossi, M.; Scalmani, G.; Rega, N.; Petersson, G. A.; Nakatsuji, H.; Hada, M.; Ehara, M.; Toyota, K.; Fukuda, R.; Hasegawa, J.; Ishida, M.; Nakajima, T.; Honda, Y.; Kitao, O.; Nakai, H.; Klene, M.; Li, X.; Knox, J. E.; Hratchian, H. P.; Cross, J. B.; Bakken, V.; Adamo, C.; Jaramillo, J.; Gomperts, R.; Stratmann, R. E.; Yazyev, O.; Austin, A. J.; Cammi, R.; Pomelli, C.; Ochterski, J. W.; Ayala, P. Y.; Morokuma, K.; Voth, G. A.; Salvador, P.; Dannenberg, J. J.; Zakrzewski, V. G.; Dapprich, S.; Daniels, A. D.; Strain, M. C.; Farkas, O.; Malick, D. K.; Rabuck, A. D.; Raghavachari, K.; Foresman, J. B.; Ortiz, J. V.; Cui, Q.; Baboul, A. G.; Clifford, S.; Cioslowski, J.; Stefanov, B. B.; Liu, G.; Liashenko, A.; Piskorz, P.; Komaromi, I.; Martin, R. L.; Fox, D. J.; Keith, T.; Al-Laham, M. A.; Peng, C. Y.; Nanayakkara, A.; Challacombe, M.; Gill, P. M. W.; Johnson, B.; Chen, W.; Wong, M. W.; Gonzalez, C.; Pople, J. A.; *Gaussian 03*, Revision B.04 ed.; Gaussian Inc.: Pittsburgh, PA, 2003.
(43) Hay, P. J.; Wadt, W. R. *J. Chem. Phys.* **1985**, *82*, 270.
(44) Bauernschmitt, R.; Ahlrichs, R. *Chem. Phys.* **1996**, *256*, 454.
(45) Cossi, M.; Scalmani, G.; Rega, N.; Barone, V. *J. Chem. Phys.* **2002**, *117*, 43.
(46) Tomasi, J.; Cammi, R.; Mennucci, B.; Cappelli, C.; Corni, S. *Phys. Chem. Chem. Phys.* **2002**, *4*, 5697.
(47) Biswas, N.; Kapoor, S.; Mahal, H. S.; Mukherjee, T. *Chem. Phys. Lett.* **2007**, *444*, 338.
(48) Cornard, J. P.; Lapouge, C. *J. Phys. Chem. A* **2004**, *108*, 4470.
(49) Kiss, T.; Nagy, G.; Pécsi, M.; Kozlowski, H.; Micera, G.; Erre, L. S. *Polyhedron* **1989**, *8*, 2345.
(50) Lamy, I.; Seywert, M.; Cromer, M.; Scharff, J.-P. *Anal. Chim. Acta* **1985**, *176*, 201.
(51) Linder, P. W.; Voye, A. *Polyhedron* **1987**, *6*, 53.
(52) Shimoni-Livny, L.; Glusker, J. P.; Bock, C. W. *Inorg. Chem.* **1998**, *37*, 1853.
(53) Jarzecki, A. A. *Inorg. Chem.* **2007**, *46*, 7509.

JP805463P